POLAR NEPHELOMETER FOR ATMOSPHERIC PARTICULATE STUDIES

M. Z. HANSEN AND W. H. EVANS

SUBMITTED TO APPLIED OPTICS

The majority of this work was completed while both authors were with the University of Arizona, Institute of Atmospheric Physics, Tucson, 85721. M. Hansen is presently with Goddard Space Flight Center, Laboratory for Atmospheric Sciences, Greenbelt, Maryland 20771.

A unique polar nephelometer was designed and constructed for the measurement of atmospheric particulate characteristics. The nephelometer produces visible light from a self-contained laser to irradiate an air sample drawn into the instrument. The light scattered from the particulates and molecules in the sample is detected as a function of scattering angle for each of four different incident light polarizations. These measurements are used to determine the particulate scattering matrix which is a function of the size, shape, and index of refraction of the particles. The region of sensitivity for the measurements corresponds to the size range of particles that strongly affects visible radiative transfer in the atmosphere, which is the primary application for the derived information.

I. Introduction

Atmospheric aerosol size distributions have been shown to be significant in numerous fields of study. Atmospheric particulates are essential to cloud formation, and clouds have a dominant effect on radiative transfer in the atmosphere.[1] Even for clear skies, the particulates affect the heating or cooling of the atmosphere through scatter and absorption of energy. Subsequently, the solar energy received at the surface and infrared emission into space are also affected by aerosols. These combined factors enter into the analysis of the consequences of particulates in the atmosphere. Since only minimal data are available on atmospheric aerosols, the prediction of aerosol impact on climate is severely limited.

Due to the importance of aerosols and the broad range of sizes occurring naturally and artificially, numerous techniques have been developed to measure particulate characteristics. Direct sampling is the most straightforward technique, but low counts, biased samples, and slow analysis leave much to be desired. Nuclepore filters[2] have been used for sizing the smaller particles (below 0.1 μm in radius). Knollenburg counters[3] likewise measure physical size. The technique involves the occultation by particles of a collimated light source projected on an array of photodetectors. The Knollenburg counter has a dynamic range of about one order of magnitude that is set for the size range of interest down to 1 μm. Electrostatic devices such as the Whitby counter[4] utilize particulate mobility as a means of sizing aerosols. The Whitby has a usable range down to about 0.005 μm in radius. The maximum size limit is about 0.1 μm for relatively clean air such as in Tucson.

The passage of light through a medium produces scattering and absorption which is dependent on the medium's properties. Particulates scatter light according to their size, shape, index of refraction, and the wavelength, intensity and polarization of the incident light. The information encoded by the aerosol on the scattered light is a major source for aerosol analysis of particles larger than 0.1 μm. Multiwavelength radiometers which measure the extinction of the direct solar beam and solar aureole detectors which measure near forward scattered light have been used to obtain aerosol size distributions which are averaged over the entire depth of the atmosphere.[5]

Within the optically active region (where atmospheric aerosols scatter light appreciably), the size distribution and refractive index are basic parameters which can be inferred with a polar nephelometer. Typically, the terminology "nephelometer" encompasses those devices which determine particle size and/or concentration with scattered light. They are small-scale devices that incorporate their own light source. One group includes those instruments which have a wide viewing angle set at a fixed position. Both particle counters[6] and integrating nephelometers[7] fall into this category. A second group consists of polar nephelometers, which have a small field of view of scatter, but the angle at which the scatter is observed may be changed. These instruments typically measure the scatter from a single particle or from a volume element that includes many particles.[8-14]

Bistatic lidar[15] is essentially the same principle as the volume-type nephelometer. The measurements are taken, however, from scattering volumes

which may be kilometers away. Lidar has the desirable feature of being able to measure aerosols at various heights in the atmosphere, but effects such as extinction due to the long light paths and background noise must be dealt with. Also, the ability to measure scattering in the forward direction is limited due to the geometry of the system.

This paper's research encompasses the design and construction of a volume-type polar nephelometer that will determine the four elements of the Mie scattering matrix for particulates.

II. Scattering Theory

To evaluate a broad size distribution, it is necessary to sample a number of particles in an unbiased manner. The approach here is to measure the scattered light in situ from an air volume large enough to contain a statistically significant sample of particles over the range of sizes where scattering is appreciable. The scattering can be divided into two separate components for theoretical considerations, molecular and particulate.

A. Molecular Scattering

First consider the scattering from diatomic air molecules, which is well-known from Rayleigh theory. The scattering equation can be written as

$$\underline{I}_s = \underline{F}\,\underline{I}_i$$

where $\underline{F}$ is the appropriate four-by-four scattering matrix and $\underline{I}$ has the units of power per unit area per unit solid angle with the underlined notation indicating a matrix. $\underline{I}_s$ represents the scattered light vector, and $\underline{I}_i$ designates the incident light vector.

The general scattering matrix for the Rayleigh case as presented by van de Hulst[16] is substituted into Eq. (1) yielding

$$\begin{pmatrix} I_l^{\wedge} \\ I_r^{\wedge} \\ U \\ V \end{pmatrix}_s = \left(\frac{2\pi}{\lambda}\right)^4 \frac{1}{r^2} \begin{pmatrix} (2A+3B)\cos^2\theta+A-B & A-B & 0 & 0 \\ A-B & (3A+2B) & 0 & 0 \\ 0 & 0 & (2A+3B)\cos\theta & 0 \\ 0 & 0 & 0 & 5B\cos\theta \end{pmatrix} \begin{pmatrix} I_l^{\wedge} \\ I_r^{\wedge} \\ U \\ V \end{pmatrix}_i . \quad (2)$$

The incident and scattered light vectors are presented in their standard Stokes polarization notation. $I_l^{\wedge}$ and $I_r^{\wedge}$ are the parallel and perpendicular radiances of the beam referenced to the plane that contains the incident and scattered light vectors. U is a measure of the plane of polarization, and V describes the ellipticity of the beam. An alternate representation uses $I = I_l^{\wedge} + I_r^{\wedge}$ for the first element and $Q = I_l^{\wedge} - I_r^{\wedge}$ for the second. r is the distance to the scatterer from the point of detection, λ is the wavelength of the incident light, θ is the scattering angle (see Fig. 1), and A and B are parameters which arise due to polarizab'lity of the nonspherical molecules. The nonspherical effect is dealt with by averaging over all possible orientations. Averaging applies quite well to the cases for nitrogen or air near standard temperature and pressure since very large numbers of molecules are in even the minimum scattering volume of the instrumental arrangement.

The depolarization ratio, $\rho = \frac{2A-2B}{4A+B}$, may be substituted into Eq. (2) giving

$$\underline{I}_s = \left(\frac{2\pi}{\lambda}\right)^4 \frac{(4A+B)}{r^2} \begin{pmatrix} (1-\rho)\cos^2\theta+\frac{\rho}{2} & \frac{\rho}{2} & 0 & 0 \\ \frac{\rho}{2} & 1-\frac{\rho}{2} & 0 & 0 \\ 0 & 0 & (1-\rho)\cos\theta & 0 \\ 0 & 0 & 0 & (1-2\rho)\cos\theta \end{pmatrix} \begin{pmatrix} I_l \\ I_r \\ U \\ V \end{pmatrix}_i \quad . \quad (3)$$

This is easily transformed [with $\underline{F}'$ representing the four-by-four matrix in Eq. (3)] to

$$\underline{I}_s = \frac{8\pi^2}{\lambda^4 r^2 N^2} \frac{3(m-1)^2}{(6-7\rho)} \underline{F}' \underline{I}_i \quad (4)$$

where m is the index of refraction for air and N is the molecular concentration. Details of this derivation are found elsewhere.[17,18] The IQUV format is more convenient for this work; therefore replace $\underline{F}'$ with

$$\underline{F}'_Q = \begin{pmatrix} \frac{1}{2}(\rho-1)\sin^2\theta+1 & \frac{1}{2}(\rho-1)\sin^2\theta & 0 & 0 \\ \frac{1}{2}(\rho-1)\sin^2\theta & \frac{1}{2}(\rho-1)\sin^2\theta+1-\rho & 0 & 0 \\ 0 & 0 & (1-\rho)\cos\theta & 0 \\ 0 & 0 & 0 & (1-2\rho)\cos\theta \end{pmatrix} \quad (5)$$

where Q indicates that the alternate terminology is in use. $\underline{I}_s$ is changed from a per molecule basis in Eq. (4) to a per unit volume (V) notation, giving

$$\underline{I}_{sv} = \frac{8\pi^2(m_t-1)^2 3NV}{\lambda^4 r^2 N_t^2 (6-7\rho)} \underline{F}'_Q \underline{I}_i \tag{6}$$

where the t subscript indicates standard values. Finally, pressure (p) and temperature (T) corrections are necessary to obtain

$$\underline{I}_{sv} = \frac{24\pi^2(m_t-1)^2 V p T_t}{\lambda^4 r^2 N_t (6-7\rho) p_t T} \underline{F}'_Q \underline{I}_i \tag{7}$$

B. Aerosol Scattering

The aerosol contribution to the scattered light is complicated because the shape of an aerosol may be highly irregular and its composition may be inhomogeneous. These factors make it difficult to theoretically calculate the scattered light from even a single particle. By making the appropriate assumptions, such as that an effective refractive index holds and that the particles behave as spheres, the tractable Mie theory can be applied to predict scattering from a collection of particles.[19] It should be noted that for radiative transfer purposes it is not essential that the particles be modeled correctly. However, it is necessary that the model produce the same effect on the incident radiation field as the actual particles do; thus, the reasoning behind such terminology as effective index of refraction. Continuing with the spherical case, one finds

$$\underline{F}_Q = \begin{pmatrix} \frac{1}{2}(M_2+M_1) & \frac{1}{2}(M_2-M_1) & 0 & 0 \\ \frac{1}{2}(M_2-M_1) & \frac{1}{2}(M_2+M_1) & 0 & 0 \\ 0 & 0 & S_{21} & -D_{21} \\ 0 & 0 & D_{21} & S_{21} \end{pmatrix} \tag{8}$$

where the matrix elements are defined by van de Hulst.[16]

Expansion in terms of the amplitude functions, S, for $\underline{F}_Q$ yields

$$\underline{F}_Q = \frac{\lambda^2}{4\pi^2 r^2} \begin{bmatrix} \frac{1}{2}(S_1S_1^*+S_2S_2^*) & \frac{1}{2}(S_2S_2^*-S_1S_1^*) & 0 & 0 \\ \frac{1}{2}(S_2S_2^*-S_1S_1^*) & \frac{1}{2}(S_1S_1^*+S_2S_2^*) & 0 & 0 \\ 0 & 0 & \frac{1}{2}(S_1S_2^*+S_2S_1^*) & \frac{1}{2}(S_1S_2^*-S_2S_1^*) \\ 0 & 0 & \frac{1}{2}(S_2S_1^*-S_1S_2^*) & \frac{1}{2}(S_1S_2^*+S_2S_1^*) \end{bmatrix} . \quad (9)$$

Designate the bracketed portion of Eq. (9) as $\underline{S}_A$ (where the subscript refers to the aerosol), and the scattered radiance for the aerosol becomes

$$\underline{I}_{sv} = \frac{\lambda^2 N_A V \underline{S}_A \underline{I}_i}{4\pi^2 r^2} \quad (10)$$

which has Eq. (6) as its molecular counterpart.

C. Total Scatter

The complete theoretical representation of the scattered light is found by combining the molecular and aerosol parts giving

$$\underline{I}_{sv} = \left(\frac{24\pi^2 (m_t-1)^2}{\lambda^4 N_t (6-7\rho)} \frac{p}{P_t} \frac{T_t}{T} \underline{F}'_Q + \frac{\lambda^2 N_A \underline{S}_A}{4\pi^2} \right) \frac{V}{r^2} \underline{I}_i . \quad (11)$$

Due to the averaging and symmetry considerations made earlier, the theoretical scattering is independent of the azimuthal angle, ϕ, and is only a function of the scattering angle (see Fig. 1). Even more generally, one can observe that the Mie scattering angular variation is similar to the Rayleigh pattern for particles whose radius is somewhat smaller than the incident light's wavelength. Unfortunately, this means that there is no

size information from small particle angular scattering. Larger particles (Fig. 2) do have distinct scattering patterns, however, which make sizing possible as $\underline{S}_A$ varies with both particle size and angle.

III. Nephelometer Design

Mie theory predicts some fraction of the incident energy at a specific wavelength for a given particle size and refractive index is scattered into a given direction. Due to previously discussed symmetry, a single 0 to 180 degree sweep totally characterizes a particulate's scattering pattern. Accordingly, if the scattered light is measured at a series of angles, information could be obtained about the particle's index of refraction and size.

Previously, it was shown that there are four unknowns in the Mie scattering matrix. Since each measurement of the scattered radiance gives a single equation with four unknowns, four independent measurements allow the solution of the scattering matrix at a given angle.

Consider the polar nephelometer which measures scattered light as a function of angle. Outside air with its particles is continuously drawn through the enclosed system by an exhaust fan (Fig. 3). In order to keep the nephelometer relatively compact, a folded light path is used from the laser to the scattering region. The 0.5145 μm line of a pulsed argon laser provides the light source, so that essentially a single wavelength is scattered from the air. A photomultiplier tube (PMT) is used to detect the radiance of light scattered by the molecules and aerosols in the field of view of the receiver optics at a given scattering angle (Fig. 4). This allows sufficient gain so that the weak scattering is above the noise level.

The scattering angle may be varied over a wide range (2 to 178 degrees), but at any one setting, only a narrow range of $\pm$.25 degrees of scattering is observed. The remaining variables are physical parameters of the aerosol itself.

For accurate scattering measurements, a number of calibration factors must be considered. The PMT integrator is gated on the laser pulse to avoid integrating noise during the off cycle of the laser. As many pulses as desired may be used to improve the signal to noise ratio since the voltage on the integrator is proportional to the light scattered onto the PMT. An LED acts as a stable light source for calibration of the PMT gain which varies (particularly for a change in supply voltage). The LED is mounted in optical contact with the PMT and produces a pulse between laser pulses which is gated and integrated in a fashion similar to the scattered light signal. The LED is temperature-controlled at 50°C with a heater, so that its output will remain virtually constant. The laser power monitor (PM) signal is likewise integrated so that any changes in energy incident on the scattering volume can be determined. (Attentuation by the scatterers is assumed negligible for purposes of this measurement.) Since this monitor signal is large, a silicone photodiode, which does not experience the same variability of sensitivity as a PMT, is used as a detector. Noise is effectively cancelled by zeroing the integrators with the laser light blocked out.

Next, the measured scattered light is corrected for changes in the scattering volume with angle, in sensitivity of the detector with distance of angle off axis, and in laser energy axially. The correction curve for

these combined factors closely follows sec θ. If P(θ), the scattering phase function, varies significantly over a given scattering volume, the problem is not as straightforward. Since the most rapid changes in P(θ) normally occur near forward scatter, a check is made by finding if

$$\frac{\sum_j v_j P(\theta_j)}{P(\theta) \sum_j v_j} \approx 1 \qquad (12)$$

at those angles (where v_j is the laser energy times the detector sensitivity for the volume element, j). When Eq. (12) holds, then $P(\theta) \sum_j v_j$ may be used as an adequate approximation where P(θ) is calculated at the angle of the central volume element. The specifics of the scattering geometry require careful attention and are covered in a rigorous manner in Hansen.[16]

The light leaves the laser linearly polarized. A polarization rotator is used to change the angle of linear polarization to any desired value. A 1/4-wave plate may be inserted into the optical path to change the polarization to circular. Values of polarization rotator angle and quarter-wave plate angle are chosen to give four independent incident light polarizations and therefore allow a unique solution for the aerosol scattering matrix elements. Subsequently, some light scatters from a sample volume and passes through a polarizer which is set at 45 degrees to the scattering plane. (The polarizer is used in front of the detector optics so that D_{21} and S_{21} appear in the radiance measurement.) The detector then gives a reading of the transmitted energy. The PMT integrator voltage (corrected for the discussed factors) is proportional to $\beta_s \underline{P}(\theta)$, the

volume scattering cross section times the phase function matrix. The values are different for aerosols and molecules so using a constant G which accounts for the terms in common gives

$$PMT = \left| G \left[\begin{matrix} \text{polarizer} \\ \text{matrix} \end{matrix} \right] [\beta_{sA} \underline{P}_A(\theta) + \beta_{sm} \underline{P}_M(\theta)] \underline{I}_i \right| . \qquad (13)$$

The PMT voltage corresponds only to the radiance magnitude element, I, which is indicated by the brackets. Pure nitrogen gas can be introduced into the nephelometer. With only nitrogen for a scatterer, the value of G may be solved as $\underline{P}_m$ and β_{sm} are determined from Rayleigh theory and β_{sA} is zero. For the case of aerosols and molecules, the value of $\beta_{sA}\underline{P}_A$ may be determined once G is known.

In summary, this instrument evaluates the aerosol characteristics through the determination of the scattering matrix at a given angle. The matrix is measured by automatically cycling the polarization of the laser light source through four different settings at the scattering angle. In the automated operation mode, measurements at successive scattering angles separated by 1, 2, 4, 8, or 16 degrees are made starting with 178 degrees scattering (Fig. 5).

During the operation of the nephelometer, the integrator voltages and scattering angle are digitized by a four and one-half digit autoranging multichannel voltmeter, then punched into paper tape. The tape is used to create either a card deck or magnetic tape file. The data are then read into a computer program which solves for the four aerosol matrix elements for each angle by simultaneous equations with the four incident light forms. Some other distinct characteristics of the system follow:

1. Only one polarization is incident on the PMT to eliminate polarization sensitivity.
2. A temperature-controlled LED is used as a gain monitor for the PMT.
3. The system is automated for data acquisition.
4. A small detector unit allows easy angular rotation for changing the scattering angle.
5. An effective light trap (made of flat polished absorbing glass) for the unscattered part of the laser beam allows large scattering angle measurements.
6. A pulsed laser is used so that peak power is high for a good S/N ratio while the laser itself is small and air-cooled.

IV. Calibration

To verify the proper operation of the system and to calibrate the nephelometer, the system was sealed and flushed with filtered air, then nitrogen gas. This procedure lowered particulate counts in the nephelometer to below the measurable level of an expansion-type counter (less than 50 particles per cubic centimeter). Measurements of scattering that were subsequently taken showed reasonable agreement with the expected molecular scattering (Figs. 6 and 7). Errors of 1 to 2 percent were observed at angles near forward and backscatter. These increased to 5 to 10 percent near 90 degrees. These values are felt to be sufficiently accurate as multiple measurements can average out the error significantly for calibration purposes. Also, since the problem is one of signal to noise and since

aerosol scattering is significantly greater in the forward direction which is of primary interest, instrumental errors less than 2 percent would be obtained. The absolute magnitude of aerosol measurements is determined by the system calibration constant obtained with the known magnitude of molecular scattering from theoretical considerations.

V. Results

Data are presented in Figs. 8-11 for particulate scattering matrix elements measured in Tucson, Arizona. The sampling location was about 10 meters above ground level. Measurements were typically made in the evening when the atmospheric conditions were more stable in order to minimize changes with time in the particulate populations. Measurement time was approximately 1 minute for each scattering angle. An expansion-type particle counter and repetition of nephelometer data were used to verify aerosol stability. Observed particle counts were typically 20,000 per cm^3, and periods of stability lasted 15 to 30 minutes.

On examination, the elements were generally observed to behave in a manner consistent with expectations. A limited amount of experimental data of a similar nature have been published.[11,13,20] Grams et al. compares most favorably as they also used atmospheric aerosols, but detailed quantitative comparisons are not valid unless simultaneous measurements are used. Curve fits are presented as a means of providing an analytical representation that follows the data reasonably well.

The M_1 and M_2 elements (Figs. 8 and 9) are fitted with a double Henyey-Greenstein function using two scaling constants. The Henyey-Greenstein function is appropriate to use for these elements due to the phase function characteristics associated with both the data and

the Henyey-Greenstein function. The double function is necessary to model both the sharp forward peak and the relatively flat backscatter region closely. An alternating gradient correction, then Gauss-Newton correction method is used to converge to a best least squares fit. Error bars are determined by a percentage of the matrix element value based on the magnitude of the radiance measurement which is strongly angle dependent. A minimum absolute error is also applied for very low values.

For the S_{21} and D_{21} elements (Figs. 10 and 11), a log formula was used for fitting the data. Sign changes were handled by taking the log of absolute values of the data, then renewing the original sign. With the data in this form, a sixth order polynomial fit was calculated. Some of the S_{21} and D_{21} values are questionable because fast changes of sign or magnitude with scattering angle are not expected for a size distribution which normally has a smoothing effect. However, these anomalies occur for low values which have the greatest percentage error. Also, the statistics for large particles are the worst due to their low numbers and large cross sections. Subsequently, variation of the large particles in the scattering volume (particularly near 90 degrees scatter) might reasonably be the cause of some irregularities.

VI. Error Analysis

Errors in the determination of size distribution from nephelometer data fall into three major categories. Sampling errors are caused mainly by obtaining a biased sample of particles. This might happen through losses in the sampling tube which channels outside air to the nephelometer.

However, the sampling tube is 8 centimeters in diameter to minimize losses. The effect due to changes in the number of very large particles in the scattering volume over the measurements in a set may also produce a bias. Forward scattering angles, where the large particles scatter strongly, have the larger scattering volumes which tend to offset this effect.

A second category of errors is designated instrumentation errors. Scattering angle error is typically less than ± 0.1 degree between the axial ray of the detector optics with respect to the axis of the laser beam. A detector acceptance angle of $\pm .25$ degree causes an additional error due to a range of accepted light scattering angles. These factors become most critical very near forward and backscatter where scattering radiance changes with angle are greatest. Errors due to optical train misalignment and PMT nonlinearities are more difficult to assess. Measurements of the PMT and integrators show errors of less than 1 percent for all except minimal measurements such as occur with molecular scatter at 90 degrees. Optics alignment is somewhat difficult to maintain. Although adjustments are made to better than 1 percent, several percent is sometimes measured at subsequent times.

Finally, data analysis itself has inherent errors. Quadrature error and other factors due to data truncation are negligible compared to other errors. The main problem is the error due to approximating real aerosols as Mie particles. This effect could easily be 10 percent and dominate the other errors, but no evaluation is attempted here.

VII. Summary and Conclusion

A polar nephelometer with a number of unique features has been developed for use in studying atmospheric aerosols. The nephelometer has sufficient sensitivity to detect molecular scatter from air. This allows the instrument to measure scattering from very clean air and to use pure molecular scattering for calibration. A relatively compact system is achieved by using a folded light path with an air-cooled argon laser for the light source. A small, sensitive detector unit permits easy angular rotation for changing the scattering angle. A narrow detector field of view of $\pm 1/4$ degree of scattering is used along with a single wavelength of incident light to minimize uncertainties in the scattering theory. The system is automated for data acquisition of the scattering matrix elements over an angular range from 2 degrees to 178 degrees of scattering. Both laser output and detector sensitivity are monitored to normalize the measured light scattering.

An analysis of molecular scattering was performed to demonstrate the instrument's capabilities. The measured particulate angular scattering elements were generally found consistent with previous measurements.

The primary need for improvement in the nephelometer design is an increase in structural rigidity and a decrease in thermal expansion effects in order to achieve a more routine operational capability. However, the results of the calibration demonstrate that realistic measurements can be made with the nephelometer. Analysis of particulate measurements will appear in a subsequent paper.

The authors would like to acknowledge Dale Hall, the electronics technician for the project. This research was funded by the Office of Naval Research under Grant Number N00014-75-C-0208.

REFERENCES

1. S. Twomey, Atmos. Environ. 8, 1251 (1974).
2. S. Twomey, J. Atmos. Sci. 33, 1073 (1976).
3. OAP-2D-GL Optical Array Spectrometer, Particle Measuring Systems, Inc., Boulder, Colo. 80301.
4. B. Y. H. Liu, K. T. Whitby, and D. Y. H. Pui, J. Air Pollution Control Assoc. 24, 1067 (1974).
5. G. E. Shaw, J. A. Reagan, and B. M. Herman, J. Appl. Meteorol. 12, 374 (1973).
6. D. D. Cooke and M. Kerker, Appl. Opt. 14, 734 (1975).
7. R. J. Charlson, W. M. Porch, A. P. Waggoner, and N. C. Ahlquist, Tellus 26, 345 (1974).
8. B. S. Pritchard and W. G. Elliot, J. Opt. Soc. Am. 50, 191 (1960).
9. A. C. Holland and J. S. Draper, Appl. Opt. 6, 511 (1967).
10. R. G. Quiney and A. I. Carswell, Appl. Opt. 11, 1611 (1972).
11. G. W. Grams, I. H. Blifford, Jr., D. A. Gillete, and P. B. Russell, J. Appl. Meteorol. 13, 459 (1974).
12. R. G. Pinnick, D. E. Carroll, and D. J. Hofmann, Appl. Opt. 15, 384 (1976).
13. R. J. Perry, A. J. Hunt, and D. R. Huffman, Appl. Opt. 17, 2700 (1978).
14. I. Kirmaci and G. Ward, Appl. Opt. 18, 3328 (1979).
15. B. M. Herman, S. R. Browning, and J. A. Reagan, J. Atmos. Sci. 28, 763 (1971).
16. H. C. van de Hulst, Light Scattering by Small Particles (John Wiley, New York, 1957).

17. M. Z. Hansen, Ph.D. Dissertation, U. Arizona (1977).

18. R. Penndorf, J. Opt. Soc. Am. 47, 176 (1957).

19. G. Mie, Ann. Phys. 25, 377 (1908).

20. A. C. Holland and G. Gagne, Appl. Opt. 9, 1113 (1970).

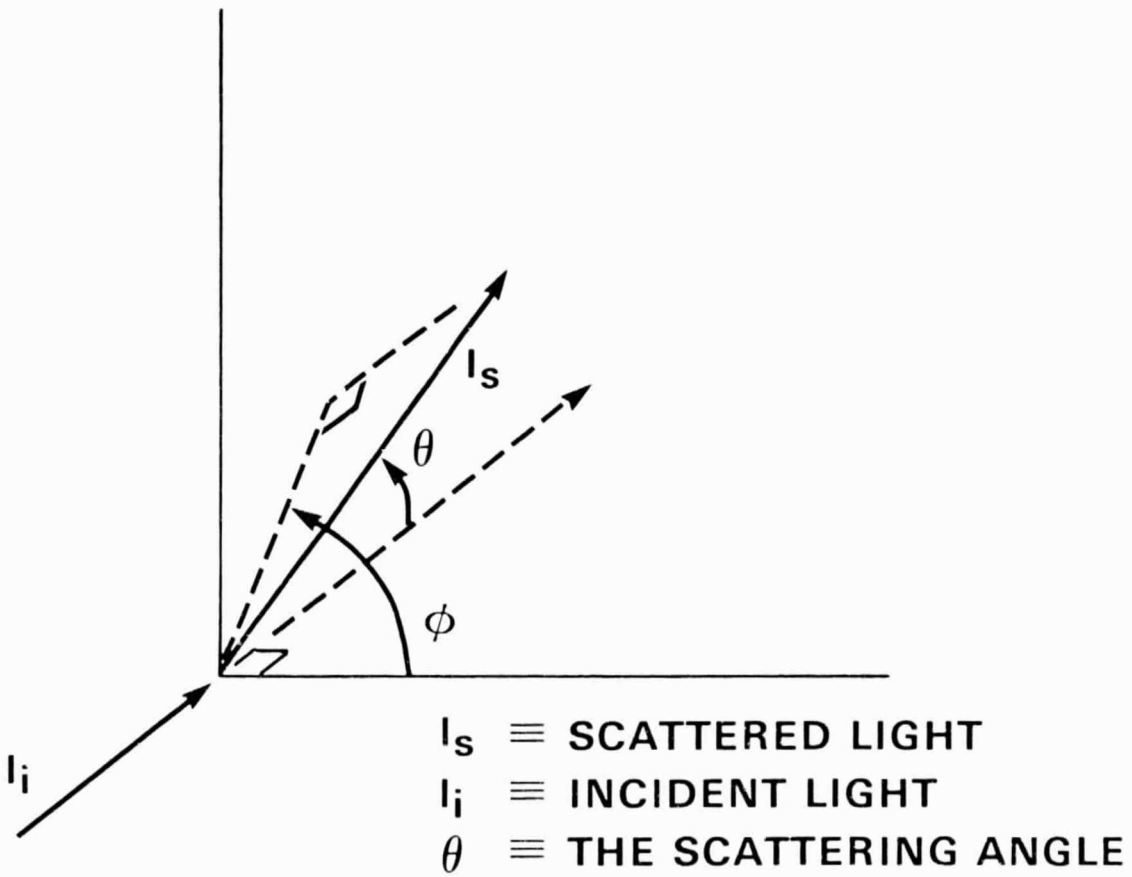

Fig. 1. Scattering angles (where ϕ is the azimuth angle of the scattered vector projected onto the transverse plane of the incident light and is measured from an arbitrarily chosen axis in the transverse plane).

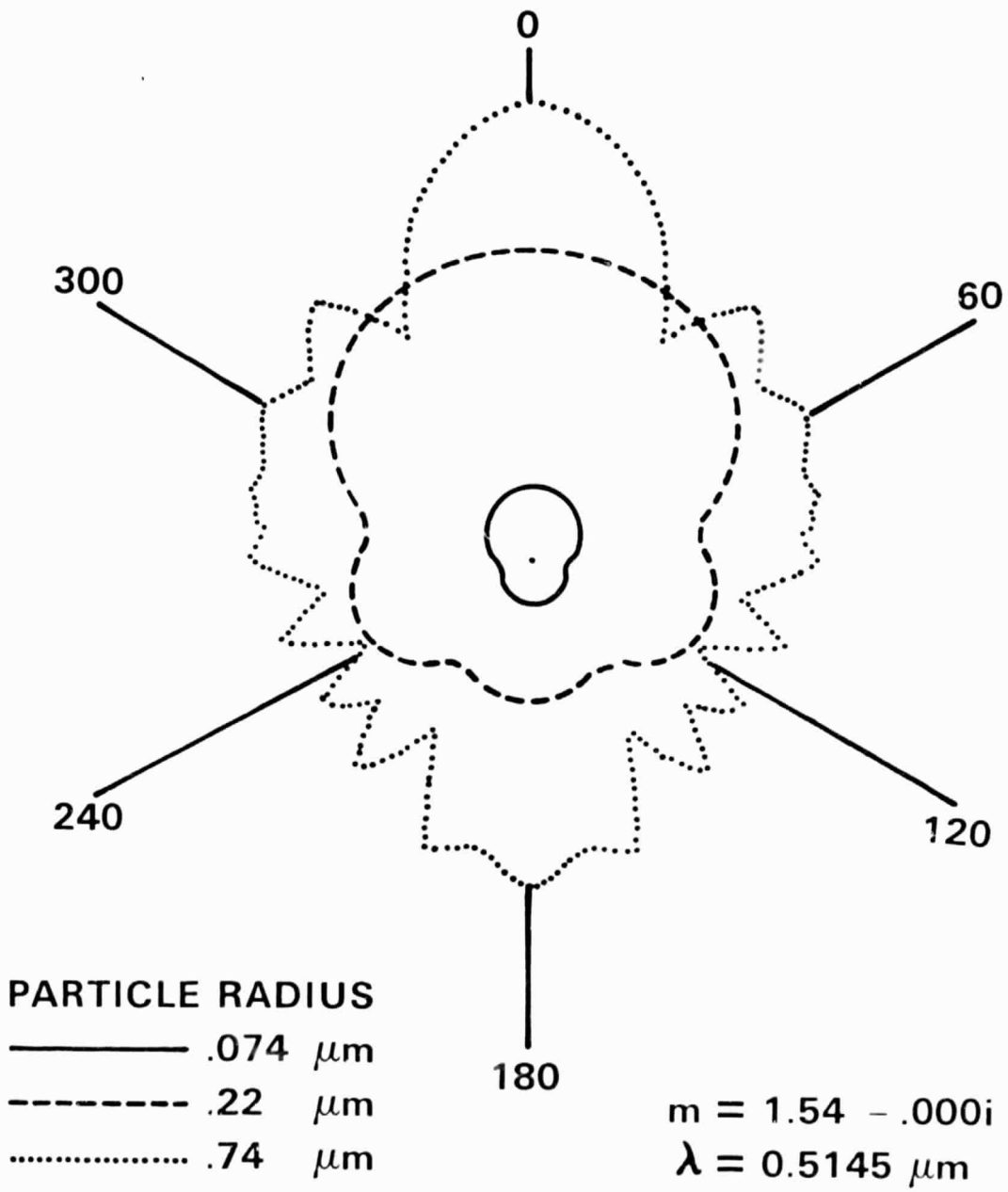

Fig. 2. Total angular radiance scattering pattern for Mie particles for unpolarized incident light.

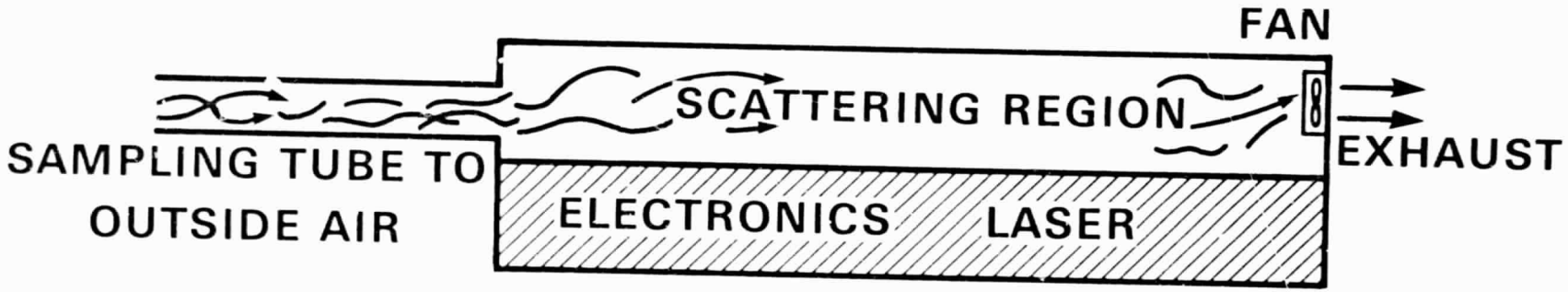

Fig. 3. Nephelometer air flow diagram.

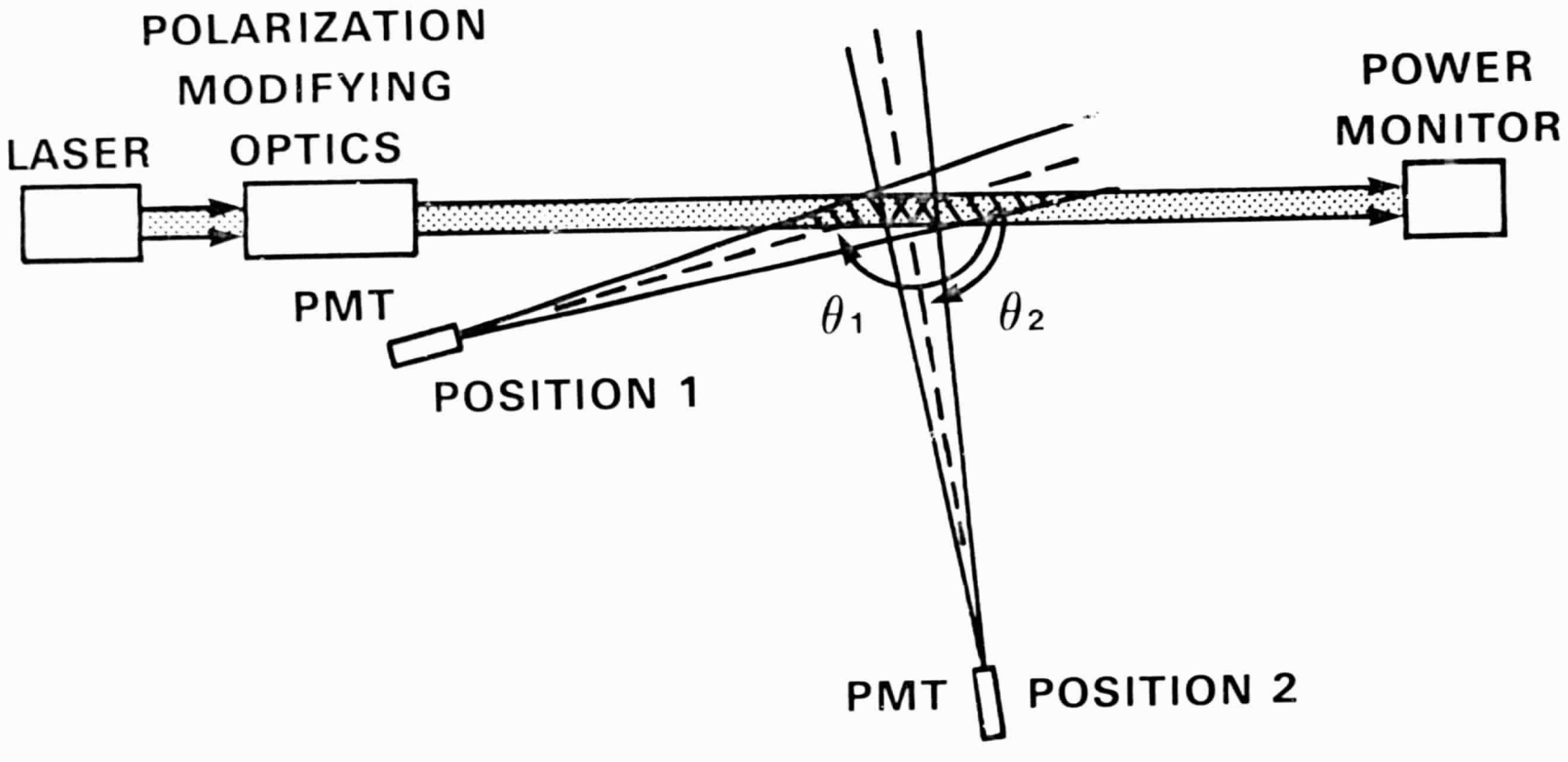

Fig. 4. Light scattering and detection schematic.

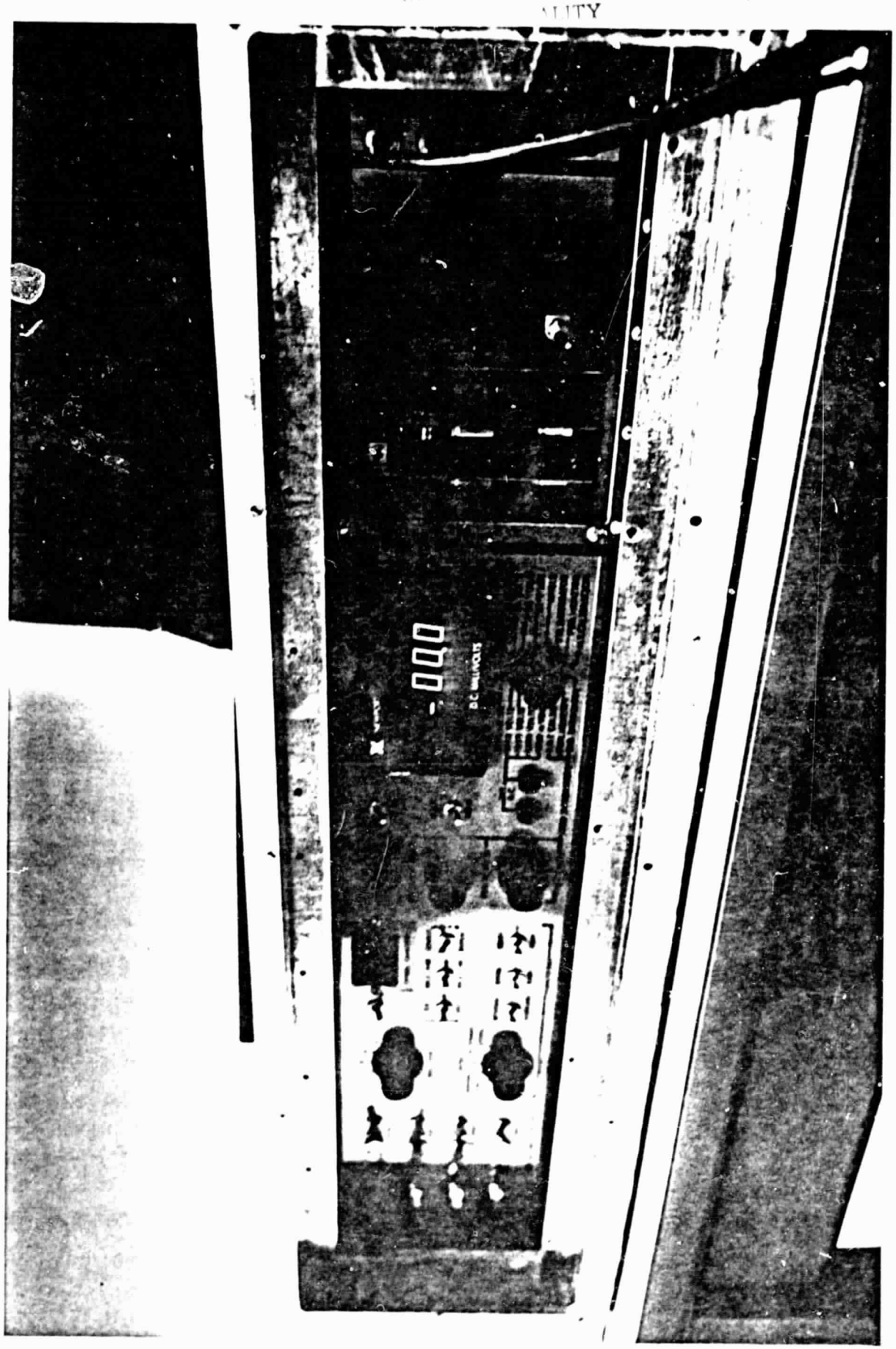

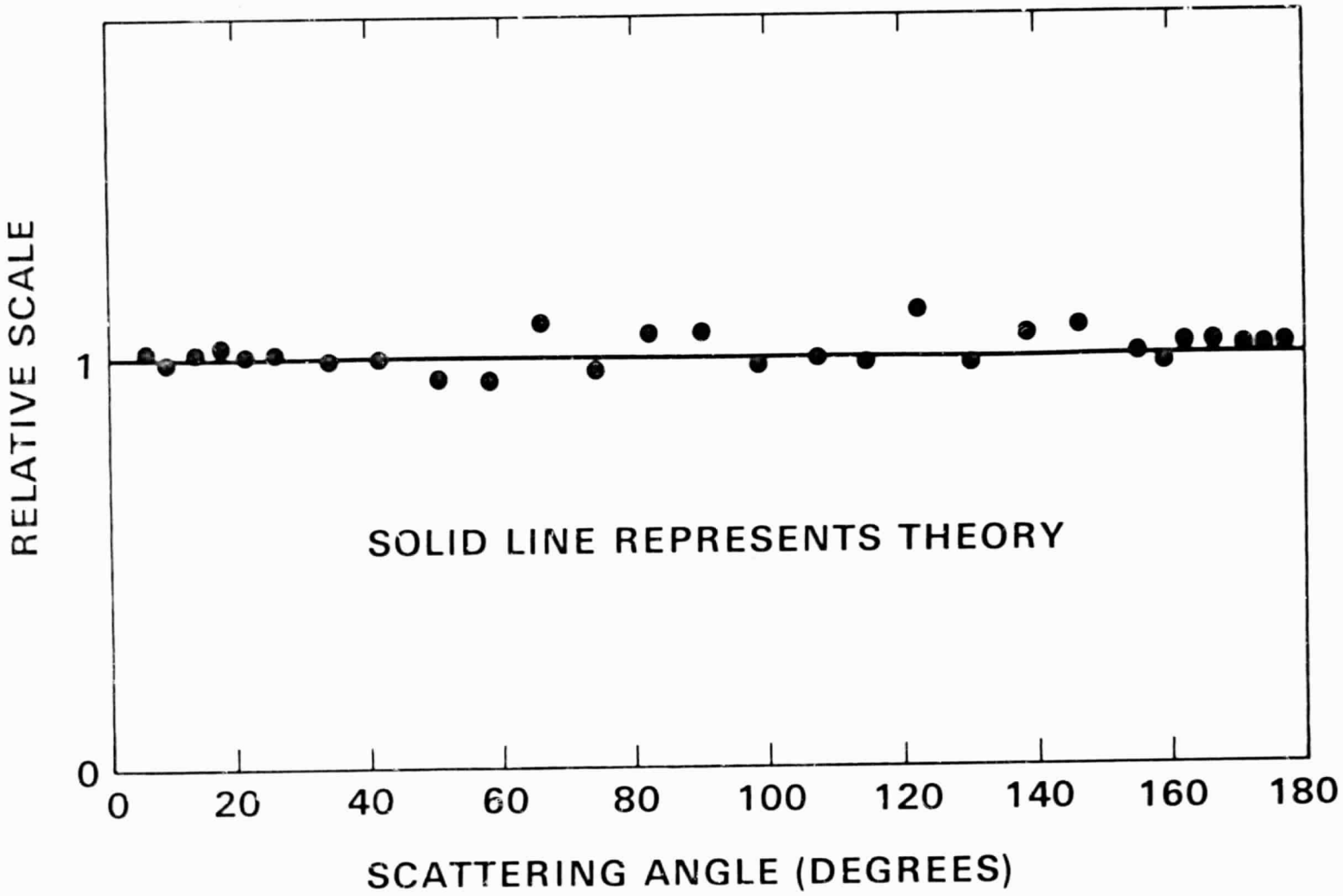

Fig. 6. Molecular scatter for perpendicular polarization of incident light.

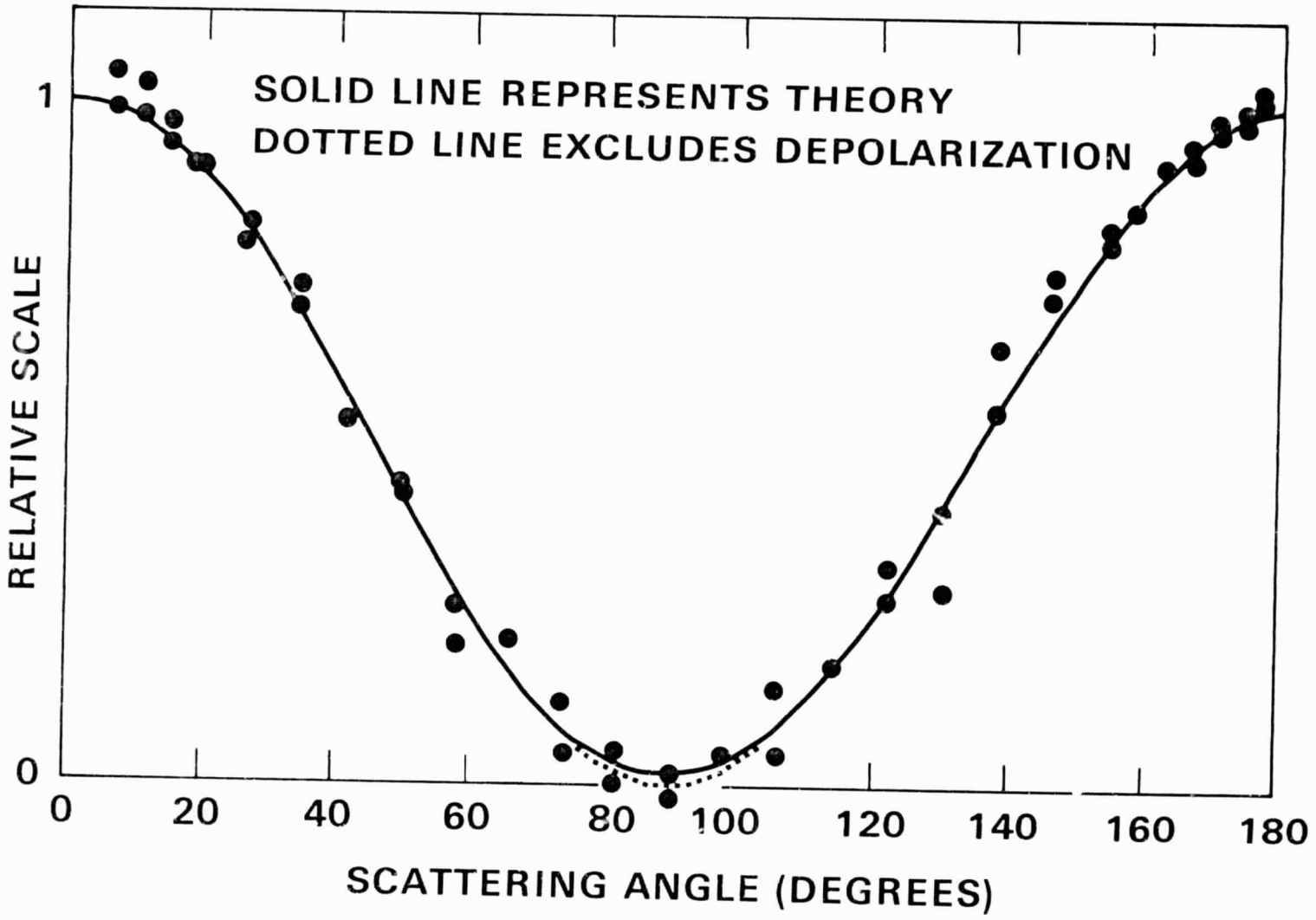

Fig. 7. Molecular scatter for parallel polarization of incident light.

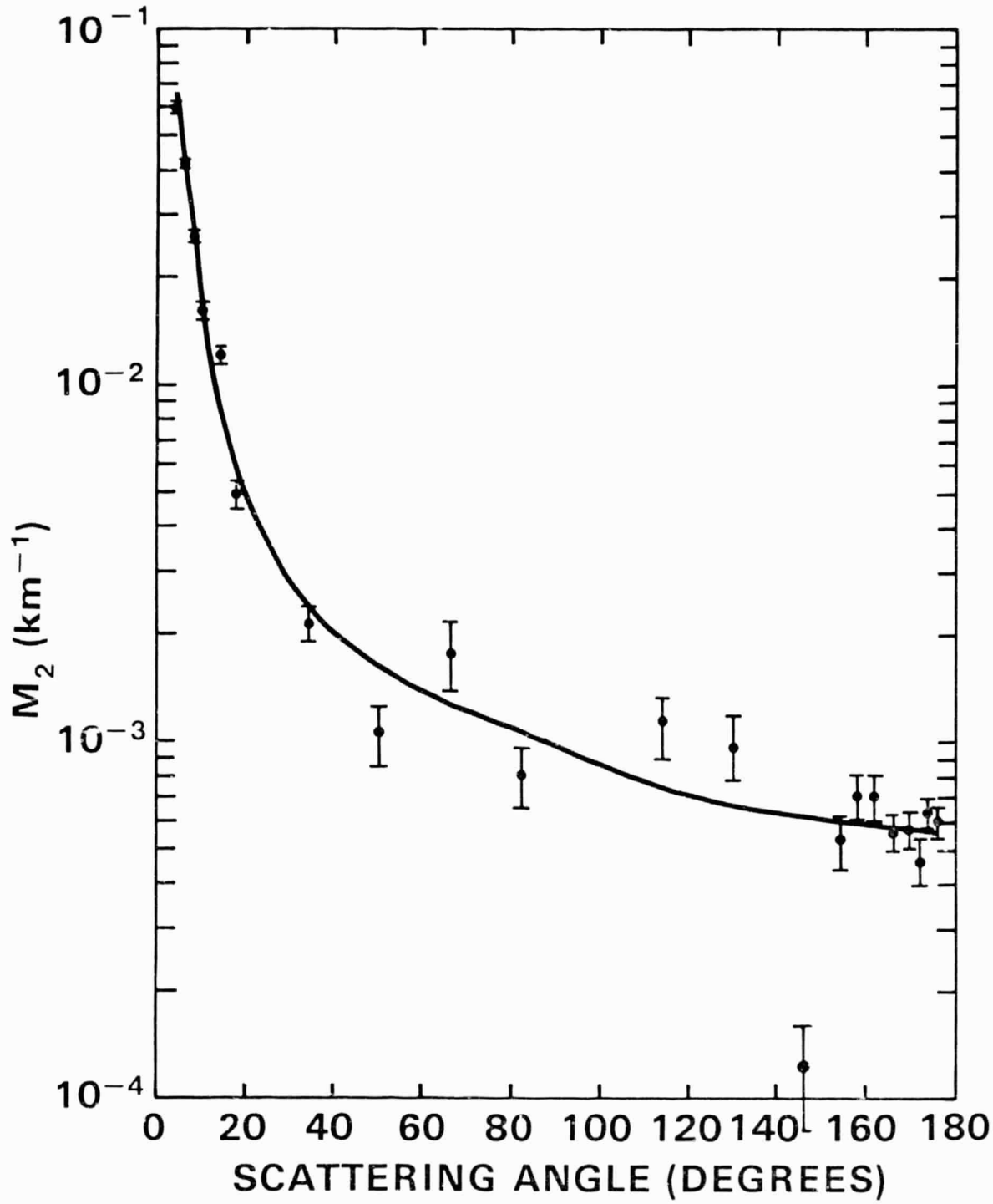

Fig. 8. M_2 matrix element for the scattering volume.

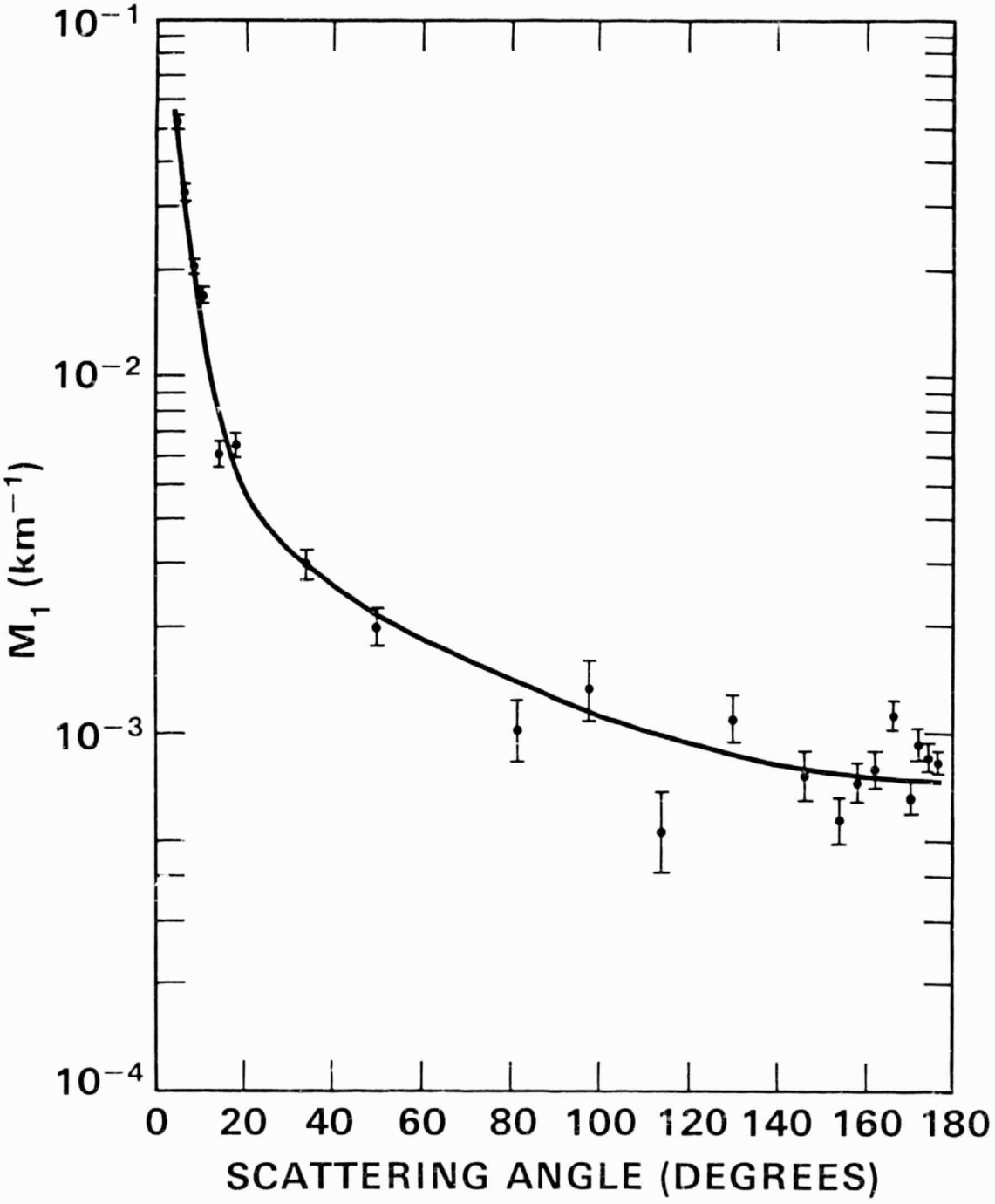

Fig. 9. M_1 matrix element for the scattering volume.

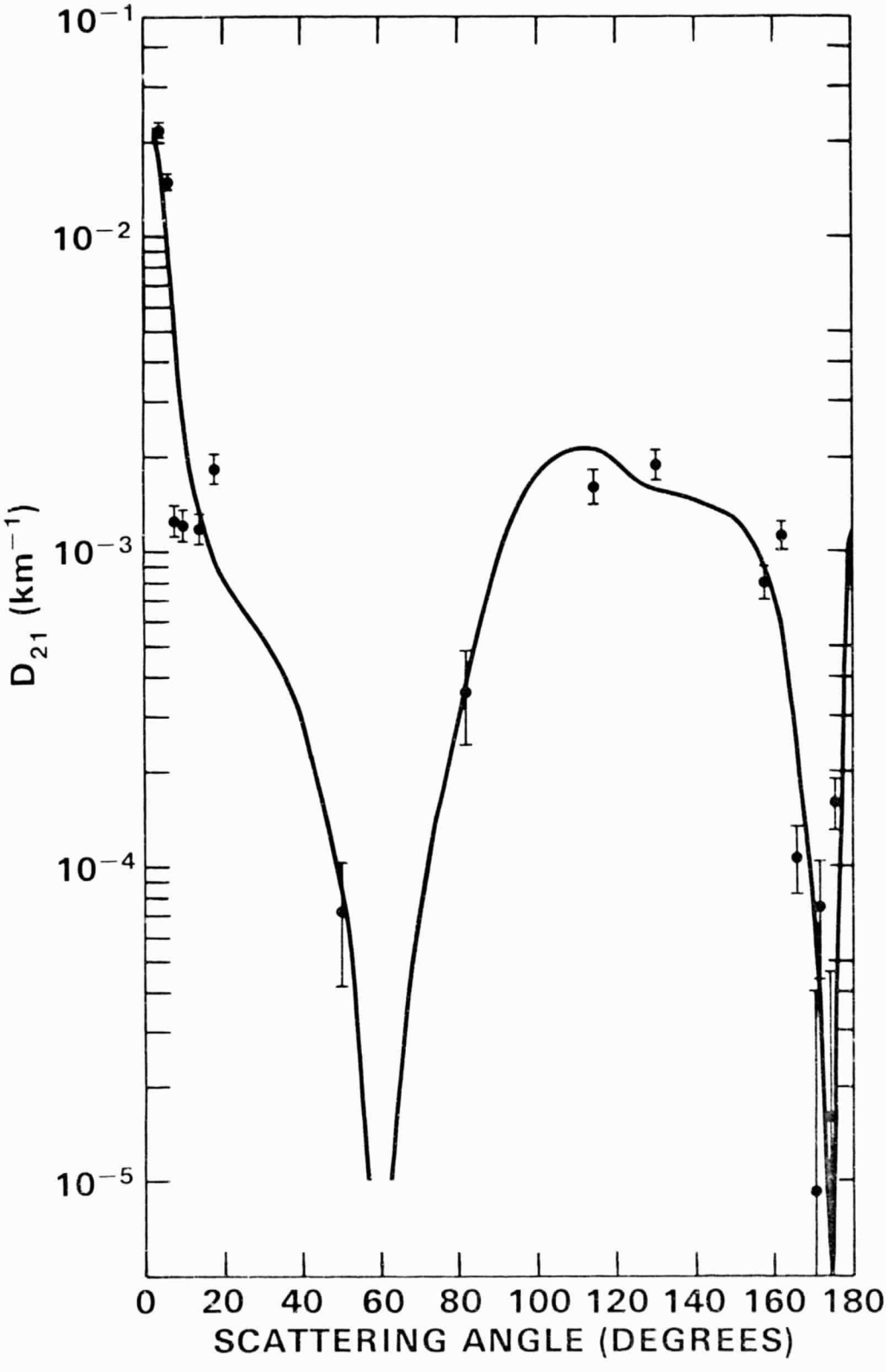

Fig. 10. D_{21} matrix element for the scattering volume.

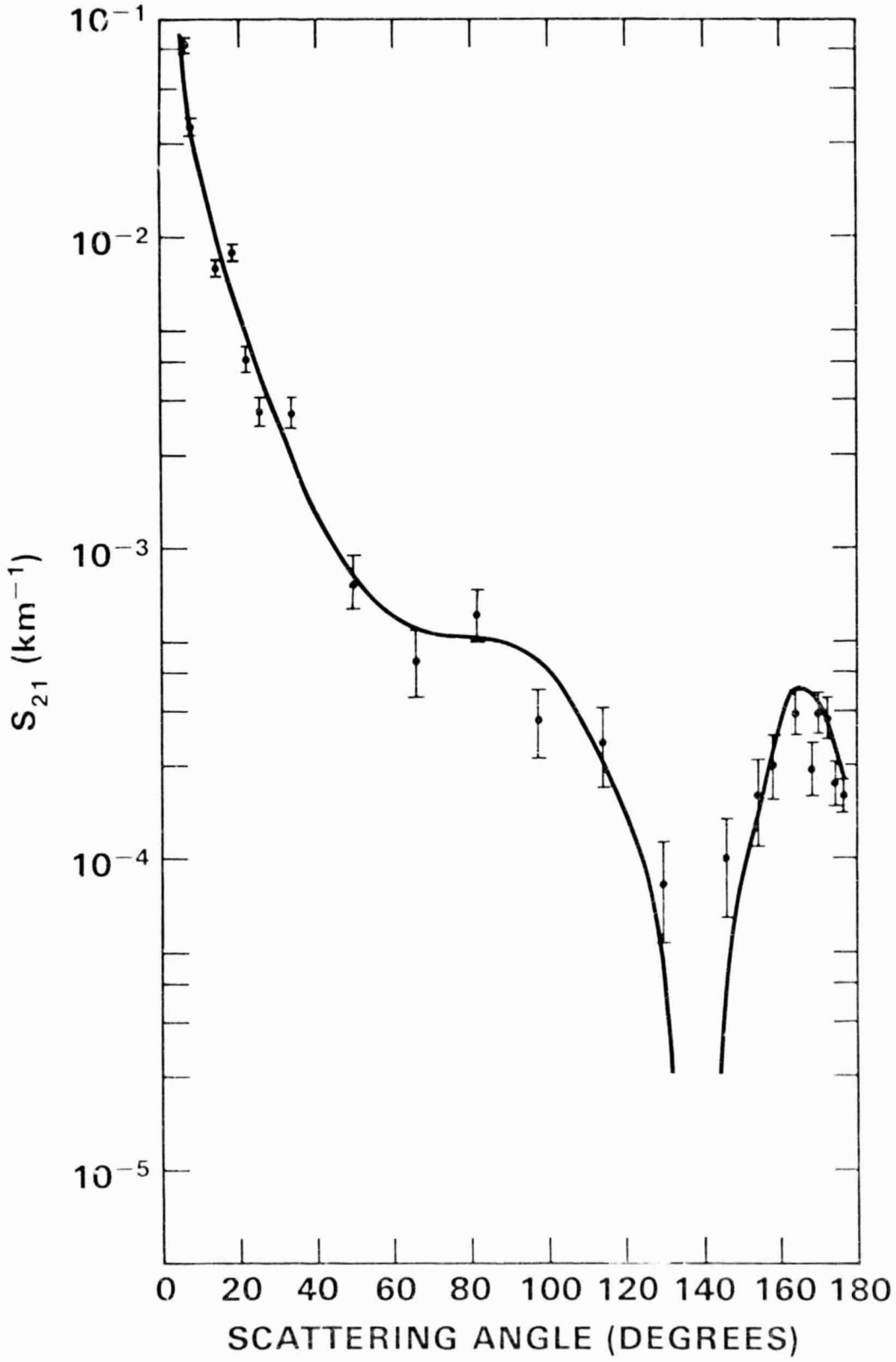

Fig. 11. S_{21} matrix element for the scattering volume.